Ceramics International xxx (xxxx) xxx–xxx

Contents lists available at ScienceDirect

Ceramics International

journal homepage: www.elsevier.com/locate/ceramint

An evaluation of the impact of crystal symmetry on microwave dielectric properties of $Sr_{1-2x}Nd_{2x}Ti_{1-x}Mg_xO_3$ solid solution

Hosein Ghobadi[a,b,*], Wen-Zhong Lu[a,b], Wen Lei[a,b], Kang Du[a,b], Fei Wang[a,b]

[a] School of Optical and Electronic Information, Huazhong University of Science and Technology, Wuhan, 430074, PR China
[b] Key Lab of Functional Materials for Electronic Information (B), Ministry of Education, Wuhan, 430074, PR China

ARTICLE INFO

Keywords:
Microwave dielectric ceramics
Nd-Mg-$SrTiO_3$ solid solutions
Near zeroτ_f
Temperature dependentτ_f

ABSTRACT

$Sr_{1-2x}Nd_{2x}Ti_{1-x}Mg_xO_3$ solid solutions for $0.05 \leq x \leq 0.30$ were prepared and their microwave dielectric (MD) properties were evaluated. Refined crystal structures showed reduced symmetries as a function of x. The tolerance factor decreased steadily and non-linearly changed the τ_f from +652.5 (x=0.10) to −28.95 (x=0.30). Raman spectra were collected to further support the less symmetrical crystal structures as well as the changes in MD properties. Oxidation state of Ti ions was investigated using XPS which presented high Ti^{4+}/Ti^{3+} ratios. A temperature dependent τ_f was observed which could be because of the variations in oxygen vacancy. Finally, the optimal properties $\varepsilon_r = 46.3$, $Q \times f = 13585$ (GHz) and $\tau_f = +2.8$ (ppm/°C) were achieved in ceramics (x=0.265) sintered at 1425°C for 3 h.

1. Introduction

The growing need for smaller wireless communication devices, such as mobile phones and satellite communication, has pushed to miniaturization of the dielectric resonator (DR) components. The main requirements for such components are a relatively high permittivity at resonance frequencies (ε_r), high quality factor ($Q \times f$) and near zero coefficient of resonant frequency (τ_f) [1]. Recently, more attention has been given to $SrTiO_3$ perovskite because of its high ε_r; however, it's high dielectric loss and large positive τ_f yet need to be reduced in order to make this ceramic applicable. Investigations into crystal structure of Ce A-site doped $SrTiO_3$ had shown reduced symmetries evident by non-cubic supercell diffractions because of the antiphase tilt of oxygen octahedra [2–5]. However, the system appears to keep its original cubic structure for small amounts of dopant [6]. Refined crystal structure revealed $R\bar{3}c$ and C2/c to be the space groups for $0.133 \leq x < 0.40$ and x=0.40 in Ce–$SrTiO_3$, respectively. Similar changes of crystal structure were observed in La–$SrTiO_3$ [2]. Unlike A-site doped $SrTiO_3$, AB-site co-doped ceramics adapt low symmetry structures at smaller dopant contents [8]. Symmetry of the perovskite structure depends on the tolerance factor [1]; therefore, AB-site co-doping can cause larger changes in tolerance factor in comparison with single site doping. Raman studies of doped $SrTiO_3$ revealed active first-order phonon modes which are normally infrared active. The polar defects, as a result of doping, change the symmetry allowing the first-order modes to be Raman active. Hardening and subsequently vanishing of the soft phonon modes in Raman spectra was detected and described as the main reason of reduced ε_r [5,9]. Properties of $SrTiO_3$ based microwave dielectric ceramics is also affected by the valence state of its constituents, mainly Ti. Majority of Ce ions in Ce–$SrTiO_3$ was shown to be in 3 + oxidation state [5], although CeO_2 was used as the initial material. Others found out that the free electrons, due to formation of oxygen vacancies, can change the valence state of Ti from 4 + to 3+ [6,7], which can deteriorate the properties. Results have shown that AB-site doping is more effective in improving the microwave dielectric properties compared to only A-site doping because co-doping eliminates the need for intentional vacancies aimed at maintaining the charge neutrality, as in case of the Ce doped ceramic. Such doping with multiple rare earth ions on A-site and Al on B-site yielded small values for τ_f ($\leq +5$ ppm/°C) and largely different values for ε_r and $Q \times f$; nevertheless, the reported sintering temperatures were rather high (≥1550°C) [10,11]. In this work we report a comprehensive study of $Sr_{1-2x}Nd_{2x}Ti_{1-x}Mg_xO_3$ solid solutions as microwave dielectric ceramics. We have deliberately chosen Nd–Mg to substitute for Sr–Ti in order to preserve the polarizability of solid solutions close to that of $SrTiO_3$, allowing for a more reliable evaluation of the impact of crustal structure, chemical composition and microstructure on microwave dielectric properties.

2. Experimental procedure

Powders were synthesized through a conventional solid-state reaction route. Stoichiometric amounts of TiO_2 (99.8%), $SrCO_3$ (99.8%),

* Corresponding author. School of Optical and Electronic Information, Huazhong University of Science and Technology, Wuhan, 430074, PR China.
E-mail address: ghobadi.hossein@yahoo.com (H. Ghobadi).

https://doi.org/10.1016/j.ceramint.2019.06.072
Received 8 May 2019; Received in revised form 6 June 2019; Accepted 8 June 2019

Nd_2O_3 (99.99%) and MgO (99.8%) were ball-milled in de-ionized water using ZrO_2 balls in a polyethylene jar. Mixtures were ball-milled separately for 5 h to yield $NdMg_{0.5}Ti_{0.5}O_3$ and $SrTiO_3$ powders, dried and calcinated at 1200°C for 5 h. Calcined powders together with 0.5 wt% B_2O_3 were re-milled for 5 h and dried over-night. Powders were mixed with 8 wt% PVA, pressed into cylindrical samples of 12 mm diameter and 6 mm height under a 150Mpa uniaxial pressure. Sintering was performed at 1300–1450°C for 3 h in air with a 5°C/min heating rate. Green compacts were fired at 550°C for 60 min to burn out the PVA. Cooling rate was 2°C/min until 1000°C which was followed by furnace cooling. Sintered samples had the compositions $Sr_{1-2x}Nd_{2x}Ti_{1-x}Mg_xO_3$ $0.05 \leq x \leq 0.30$ (0.05 increment).

Bulk densities were measured by Archimedes method. Phase composition was studied by X-ray diffractometer using CuK_α radiation (XRD-700; Shimadzu, Kyoto, Japan). Images of the polished and thermally etched surfaces were gathered using Scanning Electron Microscopy SEM (Gemini G300, Oxford instruments). Valence state of Ti was analyzed via X-ray Photoelectron Spectroscopy (AXIS-ULTRA DLD-600W, Shimadzu). Raman spectra were collected using inVia-Reflex spectrometer (Renishaw, UK). Microwave dielectric properties were measured by microwave network analyzer (Agilent E8362B, Agilent Technologies, Santa Clara, CA). A temperature range of 25–80°C was used to measure the temperature coefficient of resonant frequency (Eq. (1)).

$$\tau_f = \frac{f_{80} - f_{25}}{f_{25}(T_2 - T_1)} \times 10^6 \quad (ppm/°C) \tag{1}$$

where f_{80} and f_{25} are resonant frequencies at 80°C (T_2) and 25°C (T_1), respectively.

3. Results and discussion

Fig. 1 presents the XRD diffraction patterns of sintered samples. All samples appear to form solid solutions over the studied range of composition, as the presence of extra peaks corresponding to any secondary phases was not detected. Because of the detection limit of XRD, we also collected SEM images using back-scattered electrons (Fig. 4(h)); the same brightness for all grains is the proof of a single-phase microstructure. The XRD patterns were indexed according to a low symmetry perovskite structure analogous to the work by Cho et al. [12]. The main peaks correspond to the diffractions of a perovskite structure resembling those of $SrTiO_3$ with the low intensity half-integer reflections originating from cation ordering, cation displacement and oxygen octahedra tilt. $Sr_{1-2x}Nd_{2x}Ti_{1-x}Mg_xO_3$ can also be written in form of (1-x) $SrTiO_3$-x$Nd(Mg_{0.5}Ti_{0.5})O_3$ where for x= 0 and 1, respectively, the crystal structure is cubic and a less symmetrical perovskite (orthorhombic or monoclinic) similar to $La(Mg_{0.5}Ti_{0.5})O_3$ [8,13]. Consequently, it was expected that a solid solution of the two would result in a perovskite structure. Results of Rietveld refinement for structural parameters are listed in Table 1. Crystal structure of the solid solutions adapt lower symmetries as a function of Mg–Nd content. For x = 0.05 the structure is tetragonal which undergoes a change into orthorhombic with different space groups at higher Mg–Nd. The unit cell volume decreases which is due to the enhanced magnitude of $Ti(Mg)O_6$ octahedra tilt. Here we take the variations of the angle between two B-site cations (B–O1–B) as an indicative of the extent of octahedra tilt (Table 1). As x increases, the B–O1–B angle deviates more from 180°, meaning higher degrees of tilt for lower symmetries (inset of Fig. 1); this in turn leads to a cell contraction and reduces unit cell volume [24]. For compositions of the same crystal structure, however, the change of unit cell volume in not considerable. Moreover, the changes are less pronounced as the structure becomes less symmetrical. It can be understood that a given crystal structure can accommodate a range of Mg–Nd until the changes in cell volume is large enough to alter the space group. Fig. 2 represents the refined X-ray diffraction patterns for two compositions where a good fit is obtained for both x = 0.10 and 0.20.

Raman studies of $Sr_{1-2x}Nd_{2x}Ti_{1-x}Mg_xO_3$ system at room temperature shows first-order peaks that are absent in bulk $SrTiO_3$ (Fig. 3). Such symmetry forbidden Raman peaks were observed in thin films and nanocubes of $SrTiO_3$ because of the reduced symmetry originating from strain [14] and local tetragonality [15]. The week peak around 177 cm^{-1} in Fig. 3 corresponds toTO2 mode which vanishes for higher x. The TO4 mode around 521 cm^{-1} starts off with a strong peak and experiences a lowered intensity later. Another noticeable change in TO4 mode is the shift to higher wave numbers as a function of Mg–Nd content. Appearance of TO modes is attributed to breaking of inversion/translation symmetries similar to the results of Raman analysis in Ca-doped $SrTiO_3$ [16]. In comparison to TO4 mode, the opposite happens to LO4 where an increased peak intensity is accompanied by a shift to

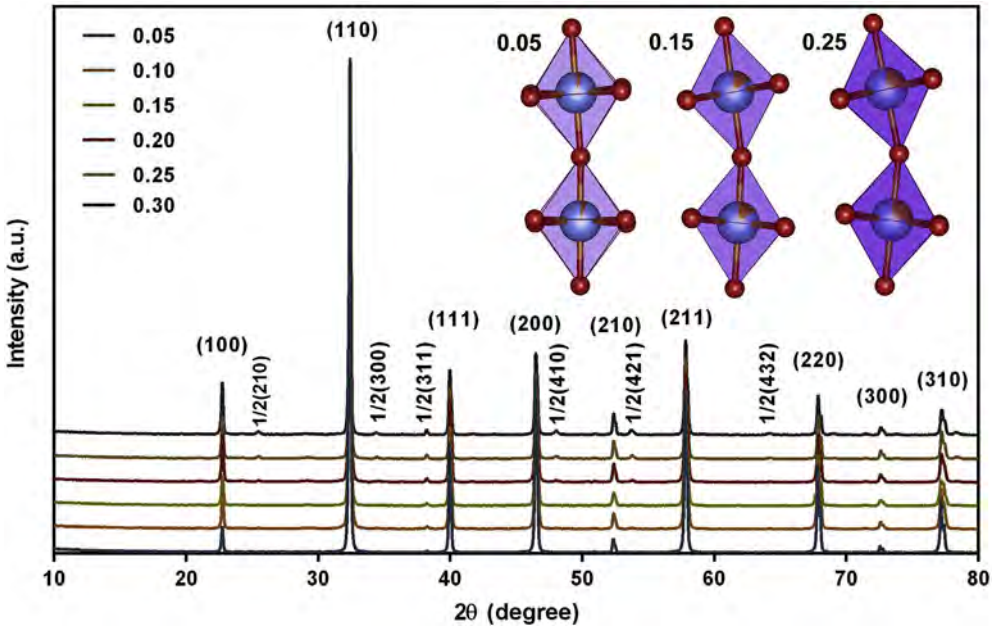

Fig. 1. X-ray diffraction patterns of ceramics sintered at 1300–1400°C. Changes in the angle of B–O1–B bonds is shown by the inset picture.

Table 1
Refined structural parameters for the compositions sintered at 1300–1450°C.

X	Unit cell parameters (Å)			Unit cell volume (Å)^3	B-site bond length (Å)	B–O1–B angle (degree)	R_{wp} (%)	Space group
	a	b	c					
0.05	5.5272	5.5272	7.8060	238.472	1.9550	174.04	10.41	I4/mcm
0.10	5.5173	7.8006	5.5311	238.048	1.9612	169.27	9.25	Imma
0.15	5.5184	7.7955	5.5331	238.026	1.9622	169.26	10.33	Imma
0.20	5.5180	5.5297	7.7990	237.970	1.9682	163.01	10.62	Pbnm
0.25	5.5180	5.5283	7.8004	237.952	1. 9690	163.01	11.31	Pbnm
0.30	5.5180	5.5280	7.8005	237.946	1.9727	162.46	11.6	Pbnm

lower wave numbers. A wide peak is characteristic of TO2, TO4 and LO4 modes because of their polar nature. Unlike polar modes, the nonpolar LO3 (Fig. 3) is characterized with a sharp peak [9]. Other first order modes are R-points of the Brillouin zone which are Raman inactive in bulk $SrTiO_3$. Reflections of these modes become intensified because of the enhanced tetragonality with x. Raman studies of Mg-doped $SrTiO_3$ below the room temperature had also shown similar changes [17]. The sharp peak at $\sim 125\,cm^{-1}$ (blue arrow) with a reduced relative intensity as a function of x originates from polar impurities and is a sign of unit cell distortion [9].

SEM micrographs at optimum sintering temperature for each composition (Fig. 4) reveal a small quantity of pores, which is a sign of relatively high densities. A relative density of > 97% was measured for almost all the compositions (Table 2). Based on SEM images, it appears that samples sintered at the same temperature, for instance x= 0.10 and 0.15, experience more grain growth as a function of Mg–Nd content. This can be explained based on solid solution nature of $Sr_{1-2x}Nd_{2x}Ti_{1-x}Mg_xO_3$ system. As far as the system stays single phase, the increased amount of Mg–Nd promotes diffusion across the grain boundaries leading to larger grains [10]; however, a limited solubility forms secondary phases at the grain boundaries hindering further grain growth [6] which was not the case in our work. Moreover, in samples sintered at higher temperatures the grain size difference increases; small grains become smaller and the large ones grow larger. As a result, the mean grain size for x= 0.265 and 0.30 is smaller than that of x= 0.20. A longer sintering time could eliminate the smaller grains through grain boundary diffusion and reduce the grain size difference, increasing the mean grain size. From the onset of doping the grains tend to adapt faceted/rectangular morphology which becomes intensified with x. Such a morphology was observed in less symmetrical ceramics [11,18] with crystal structures resembling those of this work.

Table 2 lists microwave dielectric properties along with covalency (f_c/s) calculated for each composition using equations (2) and (3)

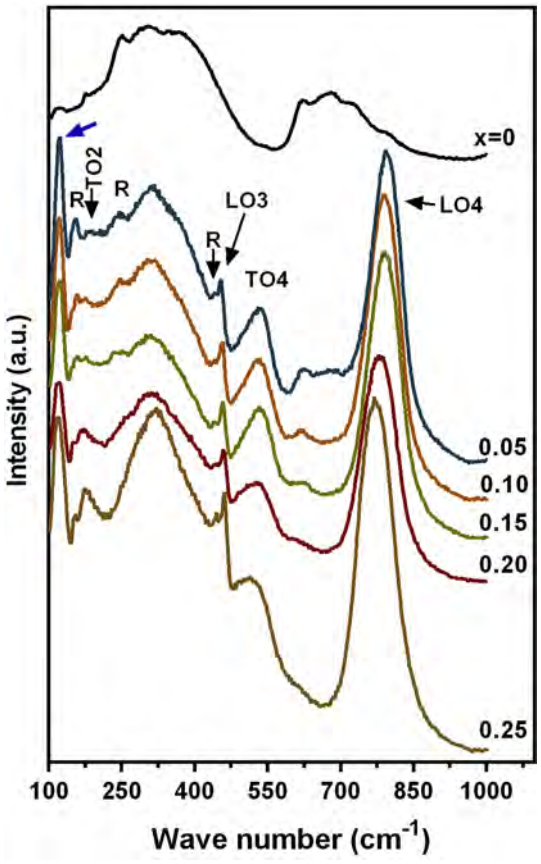

Fig. 3. Room temperature Raman spectra of $Sr_{1-2x}Nd_{2x}Ti_{1-x}Mg_xO_3$ ceramics for x= 0.00–0.25.

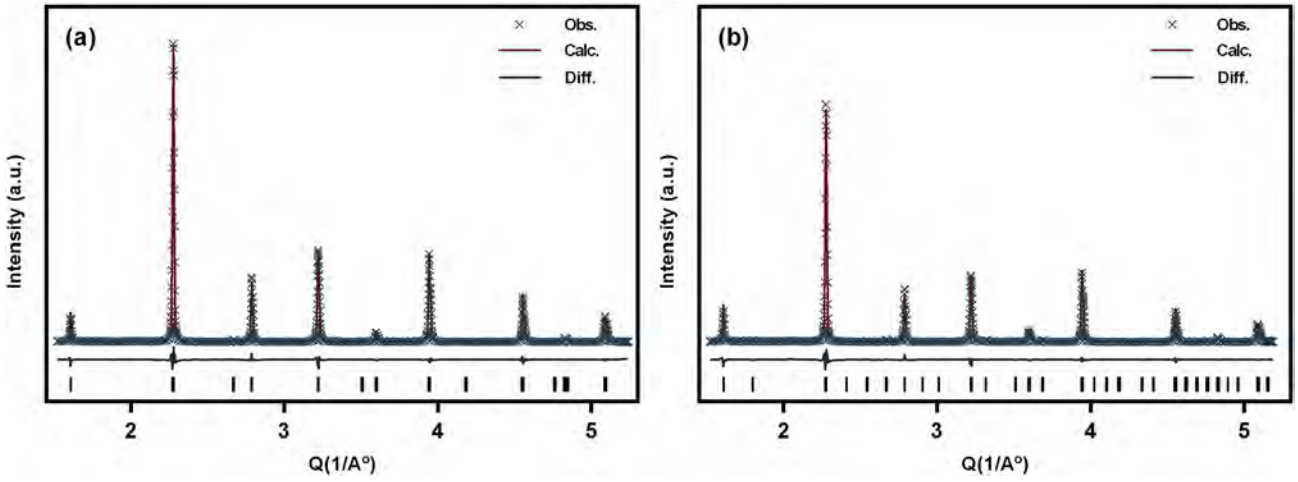

Fig. 2. Refined diffraction patterns of $Sr_{1-2x}Nd_{2x}Ti_{1-x}Mg_xO_3$ solid solutions for (a) x= 0.10 (R_{wp}=9.25%) and (b) x= 0.20 (R_{wp}=10.62%).

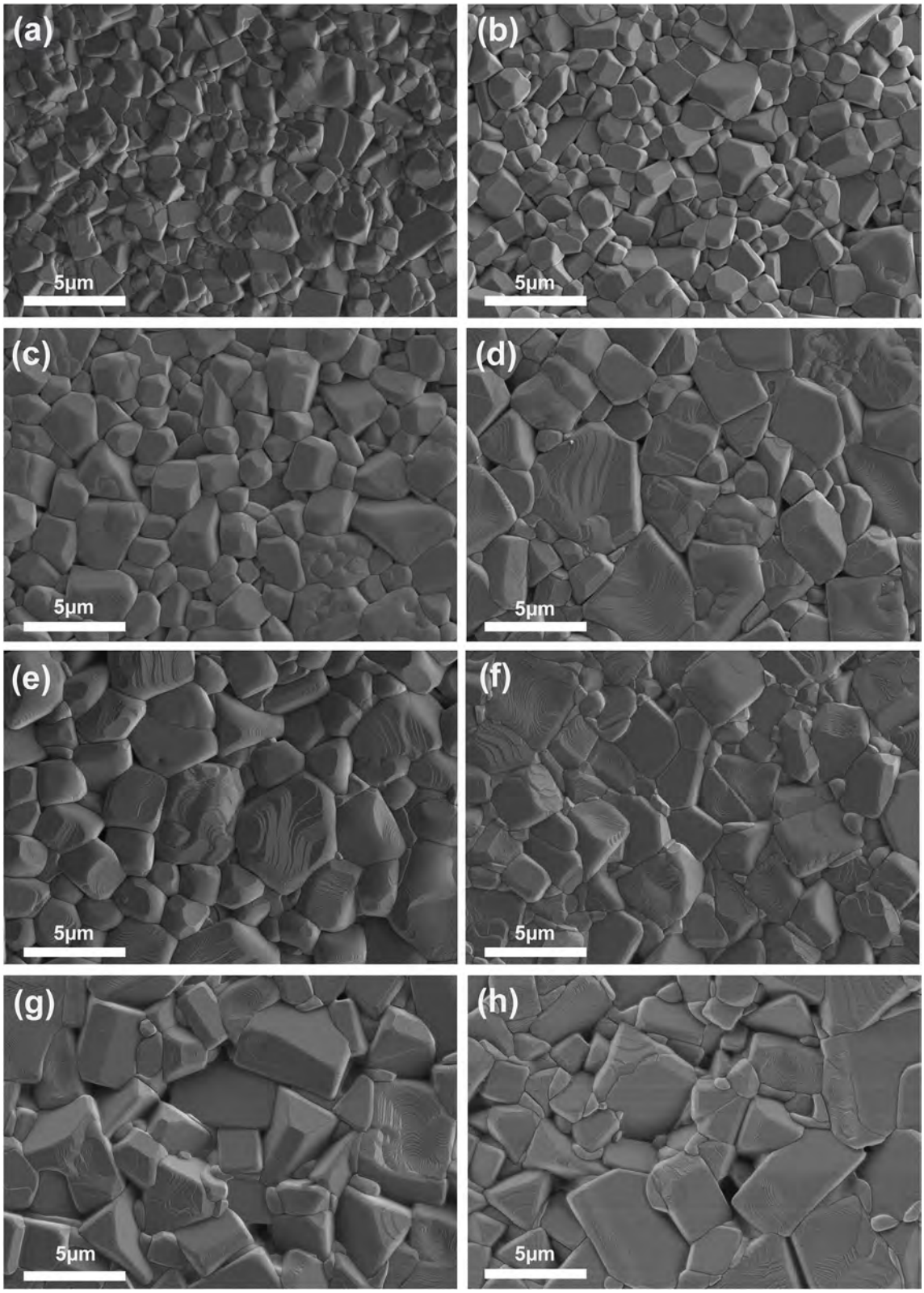

Fig. 4. Microstructure of sintered ceramics; (a) x= 0.05, (b) x= 0.10, (c) x= 0.15, (d) x = 0.20, (e) x= 0.25, (f) x= 0.265, (g) x= 0.30 and (h) backscattered electron image of x= 0.30.

proposed by I.D. Brown and R.D Shannon [19].

$$s = (R/R_1)^{-N} \quad (2)$$

$$f_c = as^M \quad (3)$$

where s is the bond strength and f_c is the covalence, R is the average bond length of Ti–O extracted from the refined data. R_1, N, a and M are empirical parameters given in Ref. [19], which for Ti, they are 1.799, 4.483, 0.49 and 1.57, respectively. The calculated covalency is reported relative to the starting composition, x= 0.05. In general, a reduced

Table 2
Microwave dielectric properties, tolerance factor and Ti–O covalency of $Sr_{1-2x}Nd_{2x}Ti_{1-x}Mg_xO_3$ solid solutions.

X	Sintering Temp. (°C)	R.D (%)	Mean grain size (μm)	ε_r	$Q \times f$ (GHz)	τ_f(ppm/°C)	Tolerance factor	$\frac{(f_c/s)_x}{(f_c/s)_{0.05}}$(%)
0.05	1300	96.88	1.88	160.5	4424	–	0.9912	100
0.10	1350	97.24	2.31	115	4673	652.5	0.9824	99.19
0.15		97.09	3.00	84	4958	395	0.9737	99.06
0.20	1400	97.12	3.96	67	8904	179	0.9651	98.29
0.25		97.08	4.10	48.4	13225	24.1	0.9565	98.19
0.265	1425	97.49	2.86	46.3	13585	2.8	0.9539	–
0.30	1450	98.34	3.67	42	15290	−28.95	0.9480	97.72

dielectric loss is expected for strongly bonded cations and anions [20,21]. Covalency of materials depends on bond strength which itself is influenced by bond length. Here, the average bond length for $Sr_{1-2x}Nd_{2x}Ti_{1-x}Mg_xO_3$ becomes larger with x which leads to a reduced covalency. Although a lowered covalency can contribute to a deteriorated quality factor, it is one of quite a few influential parameters. The intrinsic loss that depends on crystal symmetry [1] seems to play the main role here. As x increases the crystal structure adapts lower symmetries which in turn deteriorates the dielectric permittivity and, as a result, the dielectric loss. This can be explained based on Raman data (Fig. 3) where the soft phonon modes (TO2 and TO4) start to harden manifested by a shift to higher wave numbers and a reduced intensity. This diminishes the dielectric permittivity and positively impacts the quality factor [5]. Grain boundary as an extrinsic parameter is detrimental to quality factor because it can dissipate energy and is the preferred location for low melting low quality factor phases to accumulate. According to Fig. 4, the total amount of grain boundaries decreases for increased amounts of Mg–Nd which can positively affect the $Q \times f$. Nonetheless, it was shown that grain boundaries had a limited influence on quality factor of polycrystalline aluminum oxide [22]. Another influential parameter is the Ti oxidation state, with Ti^{3+} having a negative impact on $Q \times f$ because it is accompanied with oxygen vacancies. It was observed in single phase $Sr_{1-3x/2}Ce_xTiO_3$ system that quality factor steadily decreased as a function of Ce because of the elevated Ti^{3+}/Ti^{4+} ratio for the sake of preserving the charge neutrality [6]. In $Sr_{1-2x}Nd_{2x}Ti_{1-x}Mg_xO_3$ system, there is no need for charge compensation through the change of Ti oxidation state. Therefore, a low Ti^{3+}/Ti^{4+} ratio is expected as was shown by XPS surveys in Fig. 5. The Ti-$2p_{3/2}$ peak is deconvoluted into three peaks with the peak around E_B = 456.5 (eV) corresponding to Ti^{3+}. Fig. 5 shows that in both x= 0.10 and 0.30 the Ti^{3+}/Ti^{4+} ratio is not significant. A slight amount of Ti^{3+} always exists in $SrTiO_3$ because of the oxygen deficiency in sintered samples. Consequently, dependency of $Q \times f$ on changes of Ti valance state in this work should not be considerable. The difference between Ti^{3+}/Ti^{4+} ratios for x = 0.10 and 0.30 can be related to the reduced amounts of Ti^{4+} because of more substitution with Mg rather than an increase in Ti^{3+}. Variations in ε_r and $Q \times f$ of the samples are plotted in Fig. 6 (a). $Q \times f$ increases slowly for x= 0.050–0.15 that could be because of a high dielectric loss for this range of Mg–Nd. However, for x>0.15 the increase in quality factor is rapid. According to Table 2 and Fig. 6 (b), a positive correlation can be found between τ_f and tolerance factor. However, the relationship between them is not linear. The equation describing the change of τ_f is:

$$\tau_f = -\left(\frac{1}{2}\tau_\varepsilon + \alpha_l\right) \tag{4}$$

where τ_ε and α_l are the temperature coefficient of permittivity and coefficient of linear thermal expansion. Since α_l is almost constant [23], the change of τ_ε is the main determinant of τ_f, and τ_ε itself is non-linearly affected by tolerance factor. It was shown for Sr-based complex perovskites that with antiphase tilt of octahedra, τ_ε changed with a steep slope which was followed by a plateau [24]. Further reduction of tolerance factor was accompanied with in-phase tilt which only had a small effect on τ_ε. Another explanation specific to incipient ferroelectric materials such as $SrTiO_3$ is the changing magnitudes of $d\varepsilon_r/dT$ as a function of tilt transition [25]. It seems that the amplitude of change of ε_r relative to temperature becomes weaker as tolerance factor decreases. The same trend for variations of τ_ε with tolerance factor is observed in this work (Fig. 6 (b)). As tolerance factor drops to 0.9565 from 0.9912, the temperature coefficient of permittivity rapidly increases from ~ −336 to −24 (ppm/°C). Afterwards, it increases with a much slower rate for lower tolerance factors (0.9480≤ t<0.9565). Fig. 6 (c) represents the dependency of τ_f on sintering temperature for x = 0.10, 0.20 and 0.25. For most oxides, τ_f does not depend on sintering temperature. Nevertheless, in $SrTiO_3$ based ceramics the tolerance factor could be temperature dependent. A higher sintering temperature promotes Ti^{3+} and introduces more oxygen vacancies. On the one hand, Ti^{3+} (0.67A°) has a larger ionic radius than Ti^{4+} (0.605A°); thus, more Ti^{3+} is equal to a larger denominator in Eq. (5) and, consequently, a smaller tolerance factor. On the other hand, oxygen vacancies can have

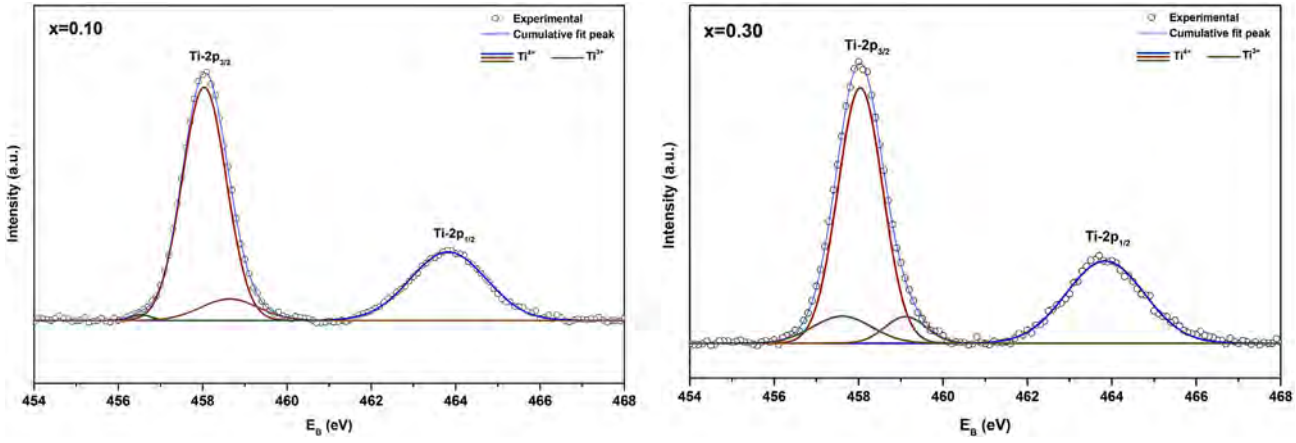

Fig. 5. Ti-2p XPS spectra for x= 0.10 and 0.30 sintered at 1400°C.

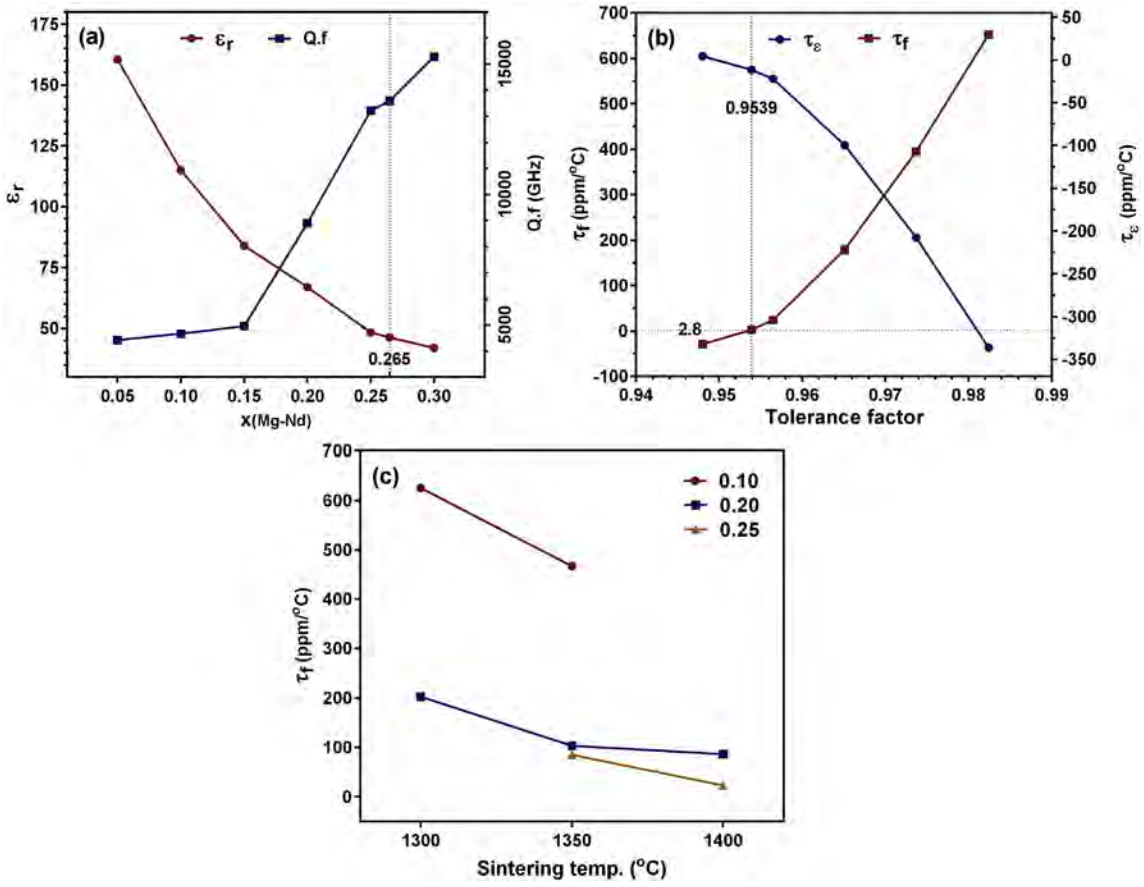

Fig. 6. Microwave dielectric properties of $Sr_{1-2x}Nd_{2x}Ti_{1-x}Mg_xO_3$ solid solutions; (a) ε_r and $Q \times f$ vs. x, (b) τ_f and τ_ε vs. tolerance factor and (c) variations of τ_f with sintering temperature.

either negative or positive impact on tolerance factor depending on the effective vacancy size. In either case, the net change appears to reduce the tolerance factor.

$$t = \frac{\bar{R}_A + R_O}{\sqrt{2}\,(\bar{R}_B + R_O)} \tag{5}$$

where $\bar{R}_A$ and $\bar{R}_B$, respectively, are the average ionic radii of cations occupying the A-site and B-site in a perovskite structure and R_O is the ionic radius of oxygen.

4. Conclusions

$Sr_{1-2x}Nd_{2x}Ti_{1-x}Mg_xO_3$ solid solutions for microwave dielectric applications were prepared and a $\tau_f = +2.8$ (ppm/°C) was obtained for $x = 0.265$. Data collected from XRD and Raman spectroscopy showed a constant decrease in symmetry as a function of x which started from the onset of substitution with Mg–Nd. These data, together with data acquired from XPS and SEM, revealed the lowered symmetry to be the main determinant of MD properties rather than polarizabilities, chemical compositions or microstructure. It was also observed that τ_f was influenced by sintering temperature because of a temperature dependent tolerance factor.

Acknowledgments

The authors appreciate the Chinese Scholarship Council (CSC) for funding this research.

References

[1] M.T. Sebastian, Dielectric Materials for Wireless Communication, first ed., Elsevier, 2008.
[2] C.J. Howard, G.R. Lumpkin, R.I. Smith, Z. Zhang, Crystal structures and phase transition in the system $SrTiO_3$–$La_{2/3}TiO_3$, J. Solid State Chem. 177 (2004) 2726–2732.
[3] R. Ubic, G. Subodh, M.T. Sebastian, D. Gout, T. Proffen, Structure of compounds in the Sr_1–3x/2CexTiO3 homologous series, Chem. Mater. 20 (2008) 3127–3133.
[4] R. Ubic, G. Subodh, D. Gout, M.T. Sebastian, T. Proffen, Crystal structure of $Sr_{0.4}Ce_{0.4}TiO_3$ ceramics, Chem. Mater. 21 (2009) 4706–4710.
[5] G. Subodh, J. James, M.T. Sebastian, R. Paniago, A. Dias, R.L. Moreira, Structure and microwave dielectric properties of $Sr_{2+n}Ce_2Ti_{5+n}O_{15+3n}$ ($n \leq 10$) homologous series, Chem. Mater. 19 (2007) 4077–4082.
[6] B. Ullah, W. Lei, Q.S. Cao, Z.Y. Zou, X.K. Lan, X.H. Wang, W.Z. Lu, Structure and microwave dielectric behavior of A-site-doped $Sr_{(1\ -\ 1.5x)}Ce_xTiO_3$ ceramics system, J. Am. Ceram. Soc. (2016) 1–7.
[7] B. Ullah, W. Lei, Z.Y. Zou, X.H. Wang, W.Z. Lu, Synthesis strategy, phase-chemical structure and microwave dielectric properties of paraelectric $Sr_{(1\ -\ 1.5x)}Ce_xTiO_3$ ceramics, J. Alloy. Comp. 695 (2017) 648–655.
[8] M. Avdeev, M.P. Seabra, V.M. Ferreira, Structure evolution in La $(Mg_{1/2}Ti_{1/2})$ O_3-$SrTiO_3$ system, Mater. Res. Bull. 37 (2002) 1459–1468.
[9] R.L. Moreira, R.P.S.M. Lobo, G. Subodh, M.T. Sebastian, F.M. Matinaga, A. Dias, Optical phonon modes and dielectric behavior of $Sr_{1-3x/2}Ce_xTiO_3$ microwave ceramics, Chem. Mater. 19 (2007) 6548–6554.
[10] F. Liu, X.Y. Liu, C.L. Yuan, J.J. Qu, G.H. Chen, C.R. Zhou, F. Liu, Microstructures and microwave dielectric properties of $(1 - x)(Sr_{0.4}Na_{0.3}La_{0.3})TiO_3$–$xLnAlO_3$(Ln = Sm, Nd) ceramic systems, J. Eur. Ceram. Soc. 35 (2015) 2091–2098.
[11] B. Ullah, W. Lei, X.Q. Song, X.H. Wang, W.Z. Lu, Phase-microstructure evolution and microwave dielectric characteristic of $(1-x)(Sr_{0.5}Ce_{0.5})TiO_{3+\delta} - xNdAlO_3$ solid solution, J. Eur. Ceram. Soc. 37 (2017) 3051–3057.
[12] S.Y. Cho, H.J. Youn, H.J. Lee, K.S. Hong, Contribution of structure to temperature dependence of resonant frequency in the (1-x)$La(Zn_{1/2}Ti_{1/2})O_3$.$xATiO_3$ (A = Ca,Sr) system, J. Am. Ceram. Soc. 84 (4) (2001) 753–758.
[13] K.W. Tay, Y.P. Fu, Q.F. Huang, F.H. Jang, Effect of Bi_2O_3 additives on sintering and microwave dielectric behavior of $La(Mg_{0.5}Ti_{0.5})O_3$ ceramics, Ceram. Int. 36 (2010) 1239–1244.
[14] A.A. Sirenko, I.A. Akimov, J.R. Fox, A.M. Clark, H.Ch Li, W. Si, X.X. Xi, Observation of the first-order Raman scattering in $SrTiO_3$ thin films, Phys. Rew. Lett. 82 (22)

(1999) 4500–4503.
[15] S. Banerjee, D.I. Kim, R.D. Robinson, I.P. Herman, Y. Mao, S.S. Wong, Observation of Fano asymmetry in Raman spectra of $SrTiO_3$ and $Ca_xSr_{1-x}TiO_3$ perovskite nanocubes, Appl. Phys. Lett. 89 (2006) 223130–223133.
[16] U. Bianchi, W. Kleemann, J.G. Bednorz, Raman scattering of ferroelectric $Sr_{1-x}Ca_xTiO_3$, x = 0.007, J. Phys. Condens. Matter 6 (1994) 1229–1238.
[17] A. Tkach, P.M. Vilarinho, A.L. Kholkin, A. Pashkin, P. Samoukhina, J. Pokorny, S. Veljko, J. Petzelt, Lattice dynamics and dielectric response of Mg-doped $SrTiO_3$ ceramics in a wide frequency range, J. Appl. Phys. 97 (2005) 044104.
[18] Y.Ch Chen, Y.H. Chang, Dielectric properties of B_2O_3-doped $La(Mg_{0.5}Sn_{0.5})O_3$ ceramics at microwave frequencies, J. Alloy. Comp. 477 (2009) 450–453.
[19] I.D. Brown, R. D Shannon, Empirical bond-strength-bond-length curves for oxides, Acta Crystallogr. A29 (1973) 266.
[20] H. Jin Jo, J.S. Kim, E.S. Kimn, Microwave dielectric properties of $MgTiO_3$-based ceramics, Ceram. Int. 41 (2015) S530–S536.
[21] S. Liu, R. Taylor, N.S. Petrovic, L. Budd, M.V. Schilfgaarde, N. Newmana, Experimental and theoretical investigation of the structural, chemical, electronic, and high frequency dielectric properties of barium cadmium tantalate–based ceramics, J. Appl. Phys. 97 (2005) 014105–014108.
[22] J.D. Breeze, X. Aupi, N.McN. Alford, Ultralow loss polycrystalline alumina, Appl. Phys. Lett. 81 (26) (2002) 5021–5023.
[23] K.H. Yoon, E.S. Kim, J.S. Jeon, Understanding the microwave dielectric properties of $(Pb_{0.45}Ca_{0.55})[Fe_{0.5}(Nb_{1-x}Ta_x)0.5]O_3$ ceramics via the bond valence, J. Eur. Ceram. Soc. 23 (2003) 2391–2396.
[24] I.M. Reaney, R. Ubic, Dielectric and structural characteristics of perovskites and related materials as a function of tolerance factor, Ferrorlrcrrics 228 (1999) 23–38.
[25] I.M. Reaney, P. Wise, R. Ubic, J. Breeze, N.McN. Alford, D. Iddles, D. Cannell, T. Price, On the temperature coefficient of resonant frequency in microwave dielectrics, Philos. Mag. A 81 (2) (2001) 501–510.